Korte, M., Constable, C., Donadini, F., Holme, R. (2011): Reconstructing the Holocene geomagnetic field. - Earth and Planetary Science Letters, 312, 3-4, 497-505

DOI: 10.1016/j.epsl.2011.10.031

Reconstructing the Holocene Geomagnetic Field

M. Korte, C.G. Constable, F. Donadini, R. Holme

April 1, 2011

Direct observations of Earth's magnetic field strength reveal a 10% decrease in dipole strength over the past 180 years, spurring discussions of whether we might be witnessing the early stage of a geomagnetic polarity reversal [e.g. 1, 2], and highlighting a need to improve reconstructions of longer term changes in the geodynamo [3]. Global geomagnetic field models spanning the past four hundred years [4] have provided a powerful tool for mapping evolving field structure at the surface of Earth's core, and are widely used for analyses of global and regional field variations. Such models have been extended to millennial time scales using global compilations of ancient field directions and intensity obtained from archaeological artifacts, lavas and sediments [see 5, for a recent review]. Despite resolution limitations, initial models *CALS3K.1* and *CALS7K.2* [6], covering the past 3 ky and 7 ky respectively, have found widespread applications in investigations of regional motions in the core [e.g. 7, 8], of the field variations known as archeomagnetic jerks [9], in providing estimates of impact of geomagnetic shielding on cosmogenic isotope production [e.g. 10, 11] and for long term data assimilation in numerical geodynamo models [12]. Here we use a comprehensive new data compilation and recently refined modelling strategies [13] to produce *CALS10k.1b*, the first time-varying geomagnetic field model spanning 10 ky. We present a new record of geomagnetic dipole evolution and of changing Holocene magnetic field morphology at

the core-mantle boundary (CMB). *CALS10k.1b* **is able to resolve mobile and structurally-evolving high latitude radial field flux lobes at the CMB in both hemispheres, as well as persistent non-zonal structure in the 10 ky average.**

Procedures for constructing *C*ontinuous models based on *A*rcheomagnetic and *L*ake *S*ediment data spanning the past *x k*y have been used in previous millennial scale models of the *CALSxk* type [13], and are briefly outlined in the Methods section. The *CALS10k.1b* model and field prediction software is available from the EarthRef Digital Archive (http://earthref.org) under the direct link http://earthref.org/***. Animation of the radial field at the CMB and the field intensity at the Earth's surface are also available there and as supplemental material to this article. The archeomagnetic data set used for *CALS10k.1b* is a previously documented compilation [14] consisting of individual directional and absolute paleointensity data and associated age information, together with estimates of their uncertainties. Sediments are represented by 75 distinct records, including calibrated relative intensity variations, and are a critical component for the extension to 10 ka. Fig. 1a shows sediment data coverage, and demonstrates key improvements over data used for the shorter *CALS7K.2* model, which relied exclusively on archeomagnetic data for intensity controls and only drew on 42 sediment records of directions. The greatly improved data coverage particularly impacts South-East Asia, Scandinavia, North and South America, the Arctic, the Mediterranean, and parts of the southern hemisphere (mainly through the calibrated intensity information). Although the data distribution is dominated by northern hemisphere data, integrated data kernels for sampling of the field at the CMB by the individual components of the data set (Fig. 1b, c and supplementary Fig. A) show complete albeit somewhat variable global coverage. Temporal coverage is also variable, as seen in Fig. 2d, because of limited length of many sediment records with high enough temporal resolution. Fewer directional data are available for the time interval 10000 BC to 7000 BC. Even more significant is a drop in relative intensity data prior to 7000 BC, with very little high-resolution information on field intensity available yet for earlier epochs. Thus even though data spanning the past 12 ky were used in constructing *CALS10k.1b*, we limit its validity to the past 10 ky. The archeomagnetic data included in the new model only play a

significant role for the time interval 0-4 ka due to their scarcity in earlier times. A variety of recent models, some providing higher spatial or temporal resolution, have focused on this shorter time-interval [15, 16, 17, 13].

CALS10k.1b is generated using bootstrap averaging (see Methods), which takes account of age uncertainties in the observations and provides a robust but low temporal resolution dipole moment prediction (Fig. 2 and supplemental data file). In common with previous lower resolution virtual axial dipole moment estimates and the *CALS7K.2* model, *CALS10k.1b* predicts relatively high values during the most recent 3 millennia and lower values before. However, the transition to the recent higher dipole moment is more gradual, and the absolute value differs. Differences in dipole moment prediction are especially significant prior to 1000 BC, where CALS7K.2 results are consistently lower than the new estimate. The timing coincides with the drop in number of archeomagnetic data, which provided the only intensity and thus dipole strength constraints in the 7 ky model. Modelling tests have confirmed that too few intensity data relative to directional data lead to underestimates of dipole moment. The new *CALS10k.1b* prediction is considered much more reliable, due to the inclusion of calibrated sediment intensity data. Note, however, that some of the sediment intensity data appear inconsistent with one another, as relatively high misfit values remain between 2500 BC and 4000 BC (Fig. 2d). Prior to 7000 BC, large misfits, a strongly increased bootstrap standard deviation, and the drop in number of data, particularly intensity, suggest that model predictions for the earliest millennium should still be viewed with some caution.

The one standard deviation uncertainty estimate for the dipole moment is about 7% on average and encompasses nearly all the faster variation predicted by the shorter but higher resolution *CALS3k.3* [16]. Somewhat surprisingly the dipole moment predicted by a more recent bootstrap average 3 ky model, *CALS3k.4b* [13] (not shown here), lies near the lower uncertainty bound. This seems to be caused by differences (ranging from -26 to +13%) in iterative re-scaling of individual sediment records that merit further investigation in future work. Field intensity predictions from the two models at the Earth's surface are quite consistent in locations with good data coverage but do show significant differences in some

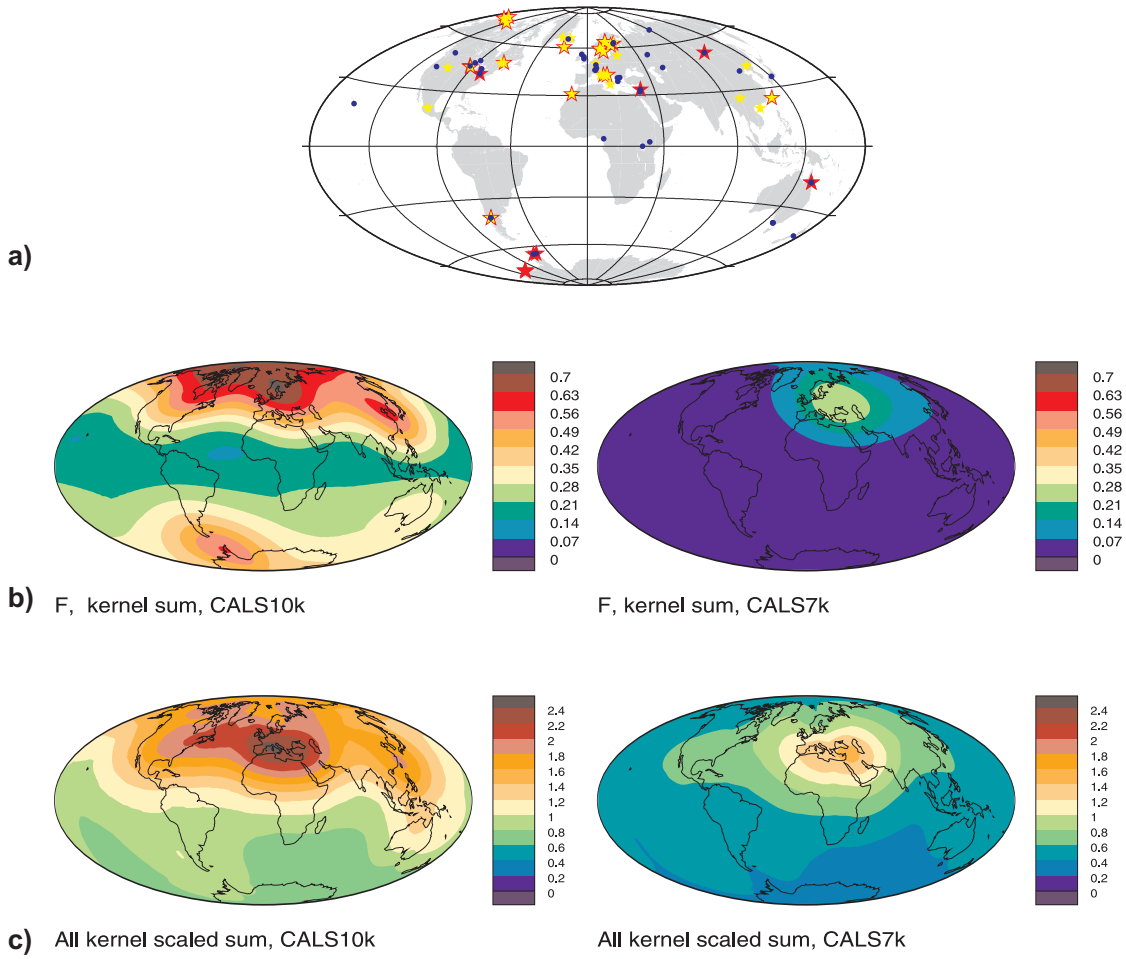

Figure 1: Data distribution and their sampling of the core field. (a) Sediment data distribution showing records added for *CALS10k.1b* compared to *CALS7K.2*, marked by yellow stars for directional data and red stars or red borders around yellow stars for calibrated relative intensity records. Locations of previously used directional records are marked in blue; (b) sampling kernels for field intensity show the cumulative relative sampling of the CMB and importance of intensity F for resolution at high latitude; (c) integrated sampling kernel for all field components for *CALS10k.1b* data distribution provides a good global sampling overall, with best coverage in mid latitude parts of the northern hemisphere. The comparison between kernels for the new model (left) and the previous *CALS7K.2* (right) demonstrates the substantial improvement in data coverage.

other regions. Again this reveals scope for improvements as new data become available in the future.

The dipole co-latitude estimate for *CALS10K.1b* (Fig. 2b and e) is consistently less throughout the Holocene than for the present field. Although the present dipole tilt seems extraordinarily large, it does lie within error estimates (typically a couple of degrees) for earlier parts of the Holocene model. Previous paleofield models agree reasonably well on magnitude of tilt, but predict significantly different dipole longitudes between 5000 and 1000 BC (Fig. 2c). This suggests that dipole longitude is quite sensitive to data distribution in the modelling, but the small error estimates obtained from the bootstraps indicate that the *CALS10k.1b* results should be robust. For much of the Holocene the geomagnetic axis was apparently located in the eastern hemisphere close to the geographic pole.

Ancient aurora sightings have previously been used for inference about past solar-terrestrial interaction. In order to estimate the strength of the solar events causing mid to low latitude aurora, the regional magnetic shielding conditions have to be considered. *CALS10k.1b* for the first time provides a consistent description of field strength and dipole tilt that allows to estimate the size and location of the auroral oval in the past. First order comparisons between dipole axis longitudes and aurora sightings at different times in Greece, Rome, the Middle East [18] and China [19] between the 7^{th} century BC and 1000 AD indicate some agreement between favourable shielding conditions and aurora sightings and invite further studies.

Almost hemispherically symmetric locations of intense magnetic flux concentrations at the core-mantle boundary (CMB) have been observed in time-averages of the historical [20] and paleomagnetic field [21, 22]. Their persistence or variability on a range of time scales is considered highly significant for a better understanding of the geodynamo processes and the influence of mantle heterogeneities [e.g. 23] in the form of thermal [24] or possibly electromagnetic [25] core-mantle coupling. Earlier millennial scale models provided tantalising, but inconclusive, results about the behaviour of high-latitude flux patches, especially in the southern hemisphere where data coverage was limited[26, 6]. A recent study revealed that although distinct southern hemisphere flux patches do not appear in

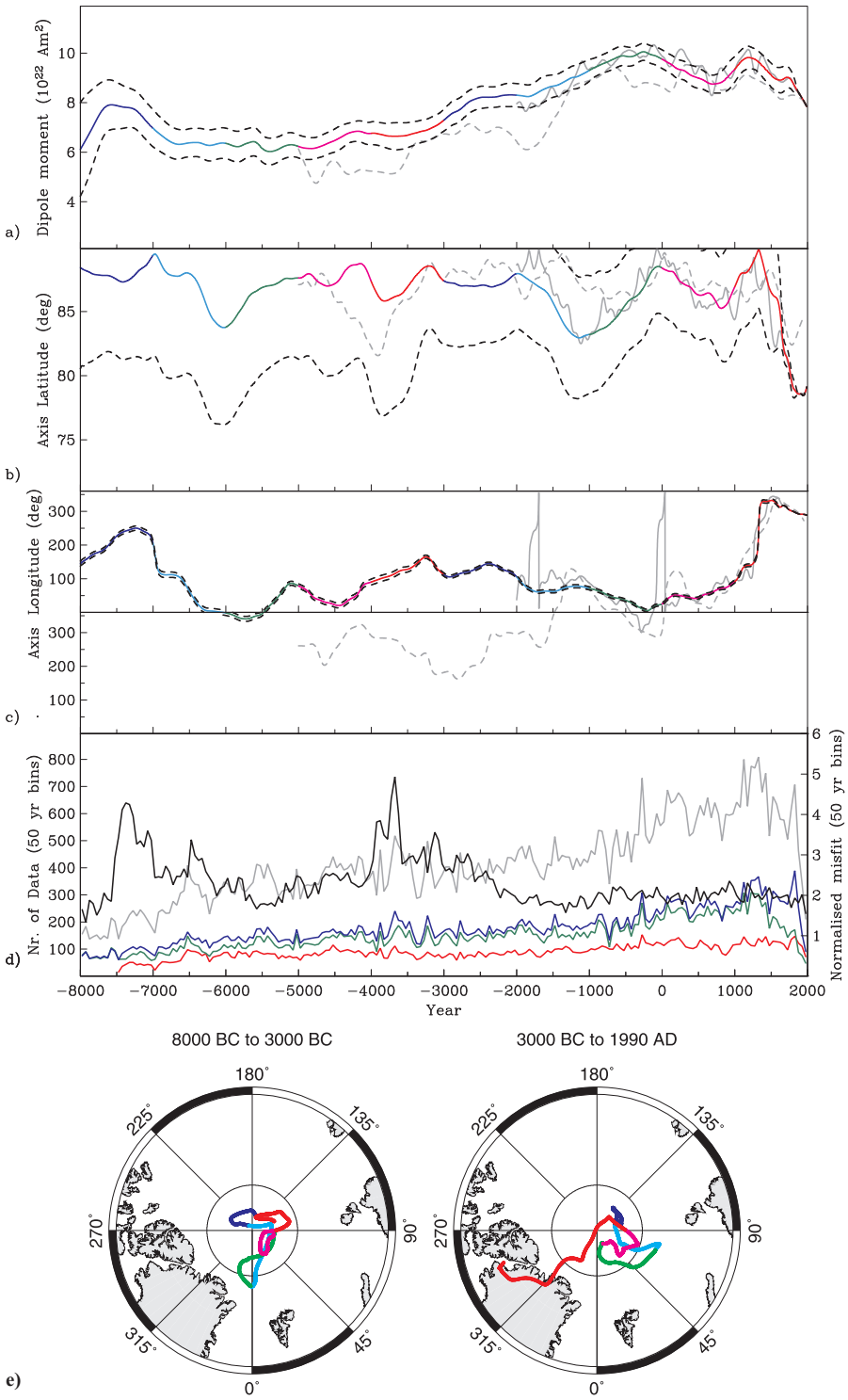

Figure 2: Dipole evolution and data distribution in time. (a) Evolution of dipole moment; (b) dipole latitude and (c) longitude for model *CALS10k.1b* (coloured line with dashed error bounds, colours refer to time intervals in panel e). Previous models also shown are *CALS7K.2* (grey dashed line) and *CALS3k.3* (gray solid line). Apparent very rapid longitudinal swings occur at times when the axis nearly coincides with the geographic pole. (d) Variability of number of available data on left axis for all data (grey), declination (green), inclination (blue) and intensity (red) and normalised misfit on right axis (black) over time. (e) Evolution of the dipole axis with time. Predominately eastern hemisphere locations are shown by *CALS10k.1b* (left: 8000 BC to 3000 BC from blue to red, right: 3000 BC to 1990 AD from blue to red.

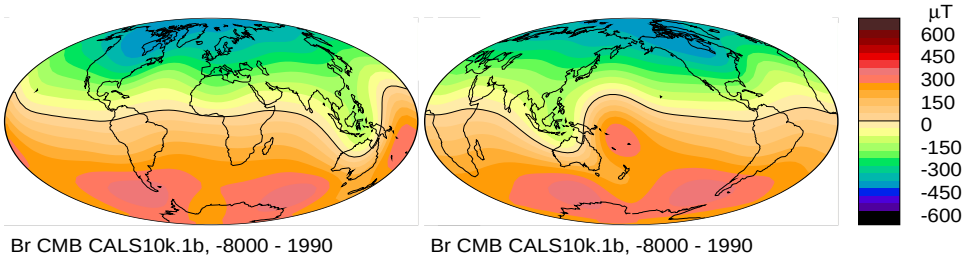

Figure 3: Time averages of *CALS10k.1b* for the radial component of the field at the core mantle boundary. Aitoff projection centred on 0 and 180°E.

the time-averaged 7 ky model *CALS7K.2*, their presence could not be ruled out with the data available at that time [27]. *CALS10k.1b* now clearly confirms the existence of two southern hemisphere regions preferentially exhibiting high-flux, which become obvious in the 10 ky average (Fig. 3). In the northern hemisphere a Canadian flux patch is obvious in the time average. The absence of a second flux patch in the Eurasian region is somewhat surprising, particularly when comparing *CALS7K.2* and the *CALS10k.1b* averaged over the same time interval (Fig. 4). Features seen in the southern hemisphere in the old and new models are generally compatible and mainly appear more pronounced in the new one. The appearance of a pronounced Canadian flux lobe in the new model can be clearly linked to the additional data, but the disappearance of two Eurasian flux patches seen in *CALS7K.2* is somewhat surprising. Some insight may be gained from the significant differences seen in a comparison of inclination anomalies at Earth's surface (Fig. 4), with large changes in inclination attributable to new Asian sediment records.

Animations of changes in the radial field at the CMB (provided in supplemental materials) confirm the high variability of both northern and southern flux patches with the number in each hemisphere varying between one and two over time. The highest flux concentrations are found just outside the tangent cylinder, with a few exceptions around 7700, 7000 and 3500 BC in the northern and between 500 BC and 200 AD in the southern hemisphere. The northern hemisphere exceptions coincide with the times of large model misfit, so that a possible distortion of flux pattern for these times by low model resolution arising from incompatible data cannot be excluded. The Holocene model therefore gen-

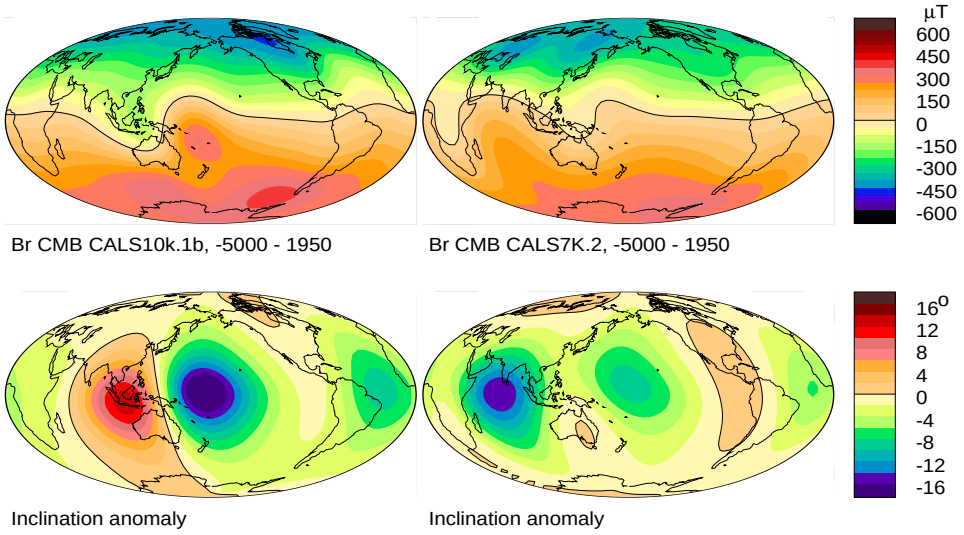

Figure 4: Comparison of time averages of *CALS10k.1b* and *CALS7K.2*, for time interval 5000 BC to 1950 AD. Shown are the radial field component at the core mantle boundary and the inclination anomaly at Earth's surface, i.e. deviation of inclination from the axial dipole.

erally supports the view of field lines concentrated at the outer boundary of the tangent cylinder by down-welling fluid and low flux at the poles associated with upwelling as seen in some numerical dynamo simulations.

The lifetime of the highest intensity patches in the *CALS10k.1b* model is typically about a thousand years throughout the Holocene. This is in general agreement with a recent study carried out on the 3 ky model *CALS3k.3* [28]. However, the higher resolution *CALS3k.3* displays additional patches of significantly shorter duration compared to the more conservative 10 ky reconstruction. Times of rather symmetric northern and southern flux concentrations (e.g. around 5700 BC or 1000 BC) alternate with times of clear asymmetries (e.g. around 7300 BC or 1000 AD). The occurrence of these strong asymmetries may support core mechanisms seen in the simulations by [23]. Vigorous convection causes significant oscillations, including the disappearance and reappearance, of flux patches about preferred locations prescribed by heat flux boundary conditions, and occasional strong drifting of patches caused by azimuthal propagation of fluid down-welling structures.

The averaged radial 10 ka magnetic field in Fig. 3 shows an additional striking feature apart from the high latitude flux patches, namely a significant undulation of the magnetic equator in the Indonesian/Australian region. Although not quite symmetric, the feature bears some resemblance to paired equatorial flux lobes observed in the recent and historical field [29]. It is the main cause of the large inclination anomalies in the Pacific and Indian oceans and surprisingly stationary from 8000 BC to about 1000 AD, mainly varying in flux intensity while the surrounding field morphology changes much more. This clearly distinguishes the feature from historical equatorial patches, which tend to show westward drift, like one particularly strong Indian Ocean patch from 1600 AD to 1990 AD [4] (which can also be seen in the *CALS10k.1b* animation due to the forced agreement with the *gufm1* historical model towards the end). Between 1100 AD and 1500 AD, when the Indian Ocean patch starts to appear, the area is devoid of strong flux concentrations. Much of the time, the southern hemisphere patch under the Pacific is stronger than the northern hemisphere counterpart. Some caution seems advisable in interpreting these structures, because the surface inclination anomalies are very large beyond regions with good data coverage. Despite good overall coverage of the equatorial CMB region (Fig. 1c) intensity data contribute relatively little to the equatorial sampling (Fig. 1b) except in the area under discussion. A similar feature, however, is observed in 5 My averages of the paleomagnetic field [21, 22] but with the southern hemisphere high intensity patch to the west of the northern hemisphere one. The western part of the feature also coincides with one of two regions where clusters of virtual geomagnetic poles (VGP) were found in transitional field lava data and is located within the preferred VGP paths for reversals [30], indicating that this might indeed be a special area in terms of field configuration and deep Earth dynamics.

We have presented the first continuous reconstruction of the Holocene geomagnetic field, allowing field predictions for any location on Earth between 8000 BC and 1990 AD. Temporal and spatial variations of millennial scale geomagnetic field models are intrinsically limited by the available data distribution and quality. Nevertheless, we have been able to map persistent non-zonal contributions to the 10 ky average field and to track the motion and persistence of individual high latitude flux patches over this time interval.

When seen in the longer term context the recent decay of the geomagnetic dipole does not appear anomalous. The associated deviation of the dipole from the geographic axis is large but should probably be viewed conservatively in light of uncertainties for earlier values and in the context of recent studies showing that the geomagnetic pole is once again on a northward track.

1 Methods

1.1 Calibration of relative intensity data

Relative intensity variations derived from sediment records have to be calibrated to absolute values before being included in the modelling. Each record is scaled by an independent constant factor based on a robust estimate of the ratio of the data to *CALS3k.3* intensity predictions at the same location. A first model was generated and the relative intensity records were iteratively re-calibrated by comparison of the data to the new model until convergence was reached [see 13, for details].

1.2 Regularised, continuous spherical harmonic model

The *CALS10k.1b* model is based on continuous magnetic field modelling techniques optimised for mapping the main field at the core-mantle boundary as pioneered by [31] and adapted for archeo- and paleomagnetic application by [6, 16, 13], where details of the method are described. The scalar magnetic potential field is expanded in spherical harmonics up to degree and order 10 in space, and in cubic B-splines with a knot-point spacing of 40 years in time and an iterative linearised fit to the data is performed. The inhomogeneity of the data set required partial steps to be taken to ensure that the algorithm converges. Physically motivated regularisations in time and space are used to find the simplest model with least structure required by the data. Regularisation norms are applied at the CMB and minimise a lower bound on Ohmic dissipation in space and of the second derivative of the radial field in time. The model parameters are summarised in supplementary table 1.

Continuous spline representations tend to exhibit unreliable end effects particularly if the data coverage becomes sparse towards the ends of the time interval. To avoid such effects at the recent end, the model has been constrained to agree with the 400-year model *gufm1* [4] from 1840 to 1990 for the axial dipole component, and from 1650 to 1990 for all other components [16, 13]. This leads to a significant increase in temporal and spatial complexity of the model for those epochs. The model parameters extend to 10000 B.C., but given the significant drop in number of intensity data prior to 8000 B.C. the validity of the model is limited to the past 10 ky.

1.3 Bootstrap average model

Data and dating uncertainties are especially significant in magnetic sediment records. The misfit is weighted by the data uncertainties, but the temporal uncertainties cannot be satisfactorily taken into account in the inversion. A relatively high resolution model (*CALS10k.1*) can be obtained by an inversion of the data set with what appear to be reasonable damping parameters by comparison of main field and secular variation power spectra [16]. Given the large uncertainties in data and dating, the presented model, *CALS10k.1b*, is an average of 2000 bootstraps on the data, preserving only robust field structure. For each of the bootstrap samples first the data are sampled from two normal distributions, one centred on the value of the magnetic component with a standard deviation corresponding to the data uncertainty estimate, and the other centred on age estimate using the respective standard error. Additionally, bootstraps on these modified data sets are performed, keeping the number of sediment records and archeomagnetic locations fixed and drawing uniformly randomly distributed records and data, respectively. Details of the method are described by [16]. *CALS10k.1b* is a rather conservative field reconstruction maintaining only the most robust spatial and temporal field characteristics and providing realistic uncertainty estimates.

References

[1] P. Olson. The disappearing dipole. *Nature*, 416:591–594, 2002.

[2] C. Constable and M. Korte. Is Earth's magnetic field reversing? *Earth Planet. Sci. Lett.*, 246:1–6, 2006.

[3] D. Gubbins, A. L. Jones, and C. C. Finlay. Fall in Earth's magnetic field is erratic. *Science*, 312:900–902, 2006.

[4] A. Jackson, A. R. T. Jonkers, and M. R. Walker. Four centuries of geomagnetic secular variation from historical records. *Phil. Trans. R. Soc. Lond. A*, 358:957–990, 2000.

[5] F. Donadini, M. Korte, and C. Constable. Millennial variations of the geomagnetic field: from data recovery to field reconstruction. *Space Sci. Rev.*, 155:219–246, 2010.

[6] M. Korte and C. G. Constable. Continuous geomagnetic field models for the past 7 millennia: 2. CALS7K. *Geochem., Geophys., Geosys.*, 6, Q02H16:doi:10.1029/2004GC000801, 2005.

[7] M. Dumberry and C. C. Finlay. Eastward and westward drift of the Earth's magnetic field for the last three millennia. *Earth Planet. Sci. Lett.*, 254:146–157, 2007.

[8] I. Wardinski and M. Korte. The evolution of the core-surface flow and changes in the length of day over the last seven thousand years. *J. Geophys. Res.*, 113, B05101:doi:10.1029/2007JB005024, 2008.

[9] Y. Gallet, G. Hulot, A. Chulliat, and A. Genevey. Geomagnetic field hemispheric asymmetry and archeomagnetic jerks. *Earth Planet. Sci. Lett.*, 284:179–186, 2009.

[10] I. Usoskin, M. Korte, and G. Kovaltsov. Role of centennial geomagnetic changes in local atmospheric ionization. *Geophys. Res. Lett.*, 35, L05811:doi:10.1029/2007GL033040, 2008.

[11] N. Lifton, D. F. Smart, and M. A. Shea. Scaling time-integrated in situ cosmogenic nuclide production rates using a continuous geomagnetic model. *Earth Planet. Sci. Lett.*, 268:190–201, 2008.

[12] W. Kuang, A. Tangborn, W. Jiang, D. Liu, Z. Sun, J. Bloxham, and Z. Wei. MoSST_DAS: the first generation geomagnetic data assimilation framework. *Comm. Comp. Phys.*, 3:85–108, 2008.

[13] M. Korte and C. Constable. Improving millennial geomagnetic field reconstructions. *Phys. Earth Planet. Int.*, submitted, 2011.

[14] F. Donadini, M. Korte, and C. Constable. Geomagnetic field for 0-3ka: 1. new data sets for global modeling. *Geochem. Geophys. Geosys.*, 10, Q06007:doi:10.1029/2008GC002295, 2009.

[15] J.-P. Valet, E. Herrero-Bervera, J.-L. LeMouël, and G. Plenier. Secular variation of the geomagnetic dipole during the past 2000 years. *Geochem. Geophys. Geosys.*, 9, Q01008:doi:10.1029/2007GC001728, 2008.

[16] M. Korte, C. Constable, and F. Donadini. Geomagnetic field for 0-3ka: 2. revised global time-varying models. *Geochem. Geophys. Geosys.*, 10, Q06008:doi:10.1029/2008GC002297, 2009.

[17] F.J. Pavón-Carrasco, M.L. Osete, J.M. Torta, and L.R. Gaya-Piqué. A regional archeomagnetic model for Europe for the last 3000 years, SCHA.DIF.3K; applications to archeomagnetic dating. *Geochem., Geophys., Geosys.*, 10:Q03013, doi:10.1029/2008GC002244, 2009.

[18] S. Silverman. Early auroral observations. *J. Atm. Solar Terr. Phys.*, 60:997–1006, 1998.

[19] M. Keimatsu, N. Fukushima, and T. Nagata. Arhaeo-aurora and geomagnetic secular variation. *J. Geomag. Geoelectr.*, 20:45–50, 1968.

[20] D. Gubbins and J. Bloxham. Morphology of the geomagnetic field and implications for the geodynamo. *Nature*, 325:509–511, 1987.

[21] C. L. Johnson and C. G. Constable. The time-averaged geomagnetic field as recorded by lava flows over the past 5 Myr. *Geophys. J. Int.*, 122:489–519, 1995.

[22] P. Kelly and D. Gubbins. The geomagnetic field over the past 5 Myr. *Geophys. J. Int.*, 128:315–330, 1997.

[23] H. Amit, J. Aubert, and G.Hulot. Stationary, oscillating or drifting mantle-driven geomagentic flux patches? *J. Geophys. Res.*, 115, B07108:doi:10.1029/2009JB006542, 2010.

[24] J. Bloxham and D. Gubbins. Thermal core-mantle interactions. *Nature*, 325:511–513, 1987.

[25] R. Holme. Electromagnetic core-mantle coupling III: laterally varying mantle conductance. *Phys. Earth Planet. Int.*, 117:329–344, 2000.

[26] C. G. Constable, C. L. Johnson, and S. P. Lund. Global geomagnetic field models for the past 3000 years: transient or permanent flux lobes? *Phil. Trans. R. Soc. Lond. A*, 358:991–1008, 2000.

[27] M. Korte and R. Holme. On the persistence of geomagnetic flux lobes in global field models. *Phys. Earth Planet. Int.*, 182:179–186, 2010.

[28] H. Amit, M. Korte, J. Aubert, C. Constable, and G. Hulot. The time-dependence of intense archeomagnetic flux patches. *??*, submitted:??, 2011.

[29] A. Jackson. Intense equatorial flux spots on the surface of the Earth's core. *Nature*, 424:760–763, 2003.

[30] K. Hoffman. Dipolar reversal states of the geomagnetic field and core-mantle dynamics. *Nature*, 359:789–794, 1992.

[31] J. Bloxham and A. Jackson. Time-dependent mapping of the magnetic field at the core-mantle boundary. *J. Geophys. Res.*, 97:19,537–19,563, 1992.

1.4 Acknowledgements

CC and FD acknowledge funding by NSF under grant number EAR 0537986 and CC under EAR 0809709. Funding for RH was provided by NERC grant NER/O/S/2003/00675.

1.5 Author Contributions

The model was produced by MK using specific millennial scale modelling strategies and data treatment developed jointly by CC and MK. RH provided additional ideas on modelling strategy and advice on some implementational aspects. FD compiled and updated the global archeomagnetic data set and helped with compiling the global set of Holocene sediment records. The initial manuscript was written by MK with improvements and some figures provided by CC.